ORGANOMETALLICS

Article

pubs.acs.org/Organometallics

Bioconjugated Rhenium(I) Complexes with Amino Acid Derivatives: Synthesis, Photophysical Properties, and Cell Imaging Studies

Vanesa Fernández-Moreira,[†] M. Lourdes Ortego,[†] Catrin F. Williams,[‡] Michael P. Coogan,[§] M. Dolores Villacampa,[†] and M. Concepción Gimeno*[,†]

[†]ISQCH-Instituto de Síntesis Química y Catálisis Homogénea, Facultad de Ciencias, Universidad de Zaragoza-CSIC, C/Pedro Cerbuna, 12, Zaragoza 50009, Spain

[‡]School of Biosciences and [§]School of Chemistry, Cardiff University, Cardiff, Wales, U.K. CF10 3AT

Supporting Information

ABSTRACT: The synthesis of a series of bioconjugated *fac* tricarbonyl rhenium bis-imine complexes with amino acid ester derivatives and their application in fluorescent microscopy cell imaging is reported. A range of *meta*- and *para*-bioconjugated pyridyl derivatives were synthesized, and their photophysical properties were analyzed upon coordination to *fac*-[Re(bipy)$(CO)_3(CF_3SO_3)$]. Their long lifetimes (270−370 ns) and large Stokes shifts (>140 nm) suggested the new bioconjugated rhenium complexes could be strong candidates for cell imaging applications. All species were taken up by MCF-7 cells and seemed to have a distinct localization pattern. However, while cells incubated with *para* derivatives had an anomalous cellular growth pattern and suffered from photobleaching upon irradiation, promoting cellular death, those incubated with the *meta* derivatives behaved in a normal manner and did not photobleach, emphasizing the importance of the ligand design when it is necessary to have an optimum outcome: i.e., cell imaging or phototherapy applications.

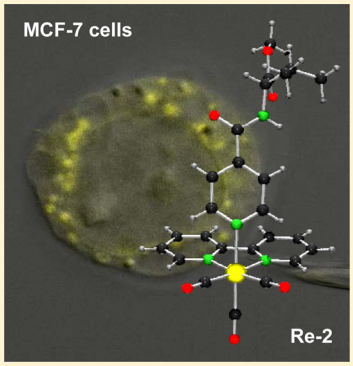

INTRODUCTION

Optimum detection of individual biomolecules, cell components, and other biological entities, as well as targeting of drugs, is becoming one of the most important issues in medicine. In order to respond to this demand, the use of luminescent visualization techniques is receiving great attention due to their noninvasive character, and consequently, there are a growing number of reports dealing with the application of phosphorescent d^6 metal complexes as luminophores in cell imaging.[1] In particular, derivatives of the *fac*-{Re^I(bis-imine)$(CO)_3$} core have attractive intrinsic photophysical properties such as large Stokes shift, long luminescent lifetimes, visible light excitation and emission, and resistance to photobleaching, among others, which make them excellent candidates for applications in cell imaging.[2] Large Stokes shifts (hundreds of nanometers) prevent self-quenching processes (reabsorption of emitted light) and allow distinguishing easily the emission of the fluorophores from the autofluorescence (emission from endogenous fluorophores, typically Stokes shift of tens of nanometers). In the same manner, long luminescent lifetime probes can be also used to filter out short-life autofluorescence via either time-gating techniques or phase-based techniques.[3] Visible light excitation and emission avoids problems of UV tissue damage, and low photobleaching character prevents the formation of nonemissive products which is normally due to the reaction of the excited state of a luminophore with oxygen. In addition to the advantageous photophysical properties of *fac*-{Re^I(bis-imine)$(CO)_3$} core, they have often also showed good biocompatibility features, such as very little or no intrinsic toxicity, stability under physiological conditions, and cell uptake and localization in different mammalian cell lines (usually human carcinoma cell lines, either HeLa or MCF-7), which can be controlled by polarity factors and/or reactivity of the ligands of the coordination sphere.[4] In this context, the introduction of biomolecules within the imaging agent seems to be an optimum approach to avoid disruption of the organism and to promote cell permeability and localization within a specific area. Conjugation of d^6 complexes to biomolecules such as estradiol, oligopeptides, peptides, and proteins is becoming a common strategy to assist in cellular uptake or to allow the sensing of other biomolecules by luminescence modulation upon interaction between these species.[5] In addition, a great number of reports have been also published dealing with the conjugation of d^6 metal complexes to biotin, which apart from their relevance in uptake processes, as biotinylated species can be actively transported into the cell, also are attractive in many biotin−avidin assays.[6] In the particular case of bioconjugated Re(I) derivatives as cellular probes, some examples of peptides[7] and different vitamin[8] and biotin[9] conjugates have been reported. However, conjugation of simpler biomolecules such amino acid derivatives and the study of their effect on cellular uptake, localization pattern, and toxicity has not, to the best of our knowledge, yet been performed. In many cases localization can be explained in terms

Special Issue: Organometallics in Biology and Medicine

Received: July 2, 2012
Published: July 30, 2012

   dx.doi.org/10.1021/om300610j | *Organometallics* 2012, 31, 5950−5957

of simple chemical processes, e.g. ionic, hydrophobic, electrostatic, and hydrogen-bonding interactions; however, in some others the picture is more complex. Incorporation of amino acid derivatives into the core structure of parent rhenium complexes should endow the novel bioconjugated species with a more friendly recognition process by mammalian cells and therefore have drastic effects on properties such as toxicity, localization, etc. Modulation of these features is an effective tool to successfully develop bioprobes suitable for different applications: i.e., cell imaging or photodynamic therapy.[10] Along that line, the study of luminescent *fac*-$\{Re^{I}(bipy)(CO)_3X\}^+$ species, where X represents a pyridyl conjugated with an amino acid derivative in *meta* and *para* positions, seems to be an optimum approach for obtaining information about the influence of such groups on the behavior of these species in vivo. The criterion for the election of the pyridyl unit over the diimine to perform the amino acid conjugation is conditioned by photophysical factors. Structural modification of the diimine unit could affect drastically the emissive properties of this type of species, as the phosphorescence observed is generally due to ^{3}MLCT transitions, specifically a $d\pi(Re) \rightarrow \pi^*$(diimine) transition. Therefore, variation of the pyridyl unit instead of the diimine will provide a feasibility study of the biological activity, whereas the luminescent properties are retained.

EXPERIMENTAL SECTION

General Measurement and Analysis. *Instrumentation.* C, H, and N analyses were carried out with a Perkin-Elmer 2400 microanalyzer. Mass spectra were recorded on a Bruker Esquire 3000 Plus, with the electrospray (ESI) technique and on a Bruker Microflex (MALDI-TOF). ^{1}H, ^{13}C{^{1}H}, and ^{19}F NMR, including 2D experiments, were recorded at room temperature on a Bruker Avance 400 spectrometer (^{1}H, 400 MHz; ^{13}C, 100.6 MHz; ^{19}F, 376.5 MHz) with chemical shifts (δ, ppm) reported relative to the solvent peaks of the deuterated solvent.[19] Room-temperature steady-state emission and excitation spectra were recorded with a Jobin-Yvon-Horiba Fluorolog FL3-11 spectrometer fitted with a JY TBX picosecond detection module. Luminescence lifetime decays were obtained using a 5000F nanosecond flash lamp and the data analyzed with the provided software package DAS6. UV/vis spectra were recorded with a 1 cm quartz cells on an Evolution 600 spectrophotometer.

Crystal Structure Determinations. Data were registered on a Bruker Smart 1000 CCD diffractometer. The crystals were mounted in inert oil on glass fibers and transferred to the cold gas stream of the diffractometer. Data were collected using monochromated Mo Kα radiation (λ = 0.710 73) in ω scans. Absorption corrections based on multiple scans were applied with the program SADABS. The structures were solved by direct methods and refined on F^2 using the program SHELXL-97.[11] All non-hydrogen atoms were refined anisotropically. Hydrogen atoms of **L2** were located in the diffraction map. Hydrogen atoms of the complex **Re-2** were included using a riding model. Further crystal data are given in Table S2 (Supporting Information). Mo Kα measured Friedel data cannot be used to determine the absolute structure in a light-atom study such as that for compound **L2**, but data for the complex **Re-2** showed unambiguously that the asymmetric carbon atoms, C20 and C50, retained, as expected, the *S* configuration of the commercial valine methyl ester used in the synthesis of **L2**.

Human Cell Incubation Studies. Human adenocarcinoma cells (MCF-7), obtained from the European Collection of Cell Cultures, Porton Down, Wiltshire, U.K., were maintained in Hepes modified minimum essential medium (HMEM) supplemented with 10% fetal bovine serum, penicillin, and streptomycin. Cells were detached from the plastic flask using trypsin-EDTA solution and suspended in an excess volume of growth medium. The homogeneous cell suspension was then distributed into 1 mL aliquots, with each aliquot being subject to incubation with a different lumophore, final concentration 100 mg mL^{-1}, at 4 °C for 30 min. Cells were finally washed three times in phosphate buffer saline (PBS, pH 7.2), harvested by centrifugation (5 min, 800*g*), and mounted on a slide for imaging. Preparations were viewed using a Leica TCS SP2 AOBS confocal laser microscope using an ×63 or ×100 objective, with excitation at 405 nm and detection at 520−570 nm.

Materials and Procedures. *fac*-[Re(bipy)(CO)$_3$(CF$_3$SO$_3$)] was prepared according to literature procedures.[12] **Re-3** and **Re-6**, specifically *fac*-[Re(bipy)(CO)$_3$(L-phenylalanine-*N*-(4-pyridylcarbonyl) methyl ester)](CF$_3$SO$_3$), and *fac*-[Re(bipy)(CO)$_3$(L-phenylalanine-*N*-(3-pyridylcarbonyl) methyl ester)](CF$_3$SO$_3$), respectively, have been prepared using a method modified from that reported in the literature for the synthesis of the analogous hexafluorophospate salts[13] (see below). All other starting materials and solvents were purchased from commercial suppliers and used as received unless otherwise stated.

General Synthesis of L1−L3. Isonicotinic acid chloride (4.08 g, 20 mmol), triethylamine (3.42 mL, 22 mmol) and the correspondent L-amino acid methyl ester (20 mmol) were stirred in dry DCM for 24 h at room temperature under an argon atmosphere. Then an aqueous solution of NaHCO$_3$ was added to the mixture and an extraction was performed (3 × 20 mL DCM). The combined organic layers were dried over MgSO$_4$ and filtered over Celite. The volume was reduced to 10 mL, and addition of hexane and/or diethyl ether afforded **L1−L3.**

*L-Alanine-N-(4-pyridylcarbonyl) Methyl Ester (**L1**).* White solid; yield 3.70 g, 89%. ^{1}H NMR (acetone-d_6): δ 8.72 (m, 2H, *H*(2)), 8.22 (s br, 1H, *NH*), 7.78 (m, 2H, *H*(3)), 4.66 (qd, *J* = 7.3, 7.3 Hz, 1H, NHC*H*), 3.70 (s, 3H, COOCH_3), 1.48 (d, *J* = 7.3 Hz, 3H, CHCH_3). ^{13}C NMR (acetone-d_6): δ 174.4 (s, 1C, COOCH$_3$), 166.6 (CONH), 152.1 (2C, *C*(2)), 142.8 (*C*(4)), 122.9 (2C, *C*(3)), 53.2 (NHC*H*), 50.3 (COOCH$_3$), 18.3 (CHCH$_3$). IR (solid, cm^{-1}): 3296 (ν(NH)), 1731 (ν(CO$_{carboxylate}$)), 1645 (ν(CO$_{amide}$)), 1537 (ν_{sym}(C═N)). Anal. Calcd for $C_{10}H_{12}N_2O_3$: C, 57.68; H, 5.81; N, 6.21; S, 13.45. Found: C, 57.42; H, 5.92; N, 6.34; S, 13,46.

*L-Valine-N-(4-pyridylcarbonyl) Methyl Ester (**L2**).* White solid; yield 4.30 g, 91%. ^{1}H NMR (acetone-d_6): δ 8.71 (m, 2H, *H*(2)), 8.05 (s br, 1H, *NH*), 7.78 (m, 2H, *H*(3)), 4.57 (m, 1H, NHC*H*), 3.72 (s, 3H, COOCH_3), 2.26 (m, 1H, C*H*-(CH$_3$)$_2$), 1.01 (2d, *J* = 6.9 Hz, 6H, CH-(CH_3)$_2$). ^{13}C NMR (acetone-d_6): δ 173.6 (COOCH$_3$), 167.4 (CONH), 152.1 (2C, *C*(2)), 143.2 (*C*(4)), 123.2 (2C, *C*(3)), 60.2 (NHCH), 53.2 (COOCH$_3$), 32.4 (CH(CH$_3$)$_2$), 20.4 (CH(CH$_3$)$_2$), 19.8 (CH(CH$_3$)$_2$). IR (solid, cm^{-1}): 3245 (ν(NH)), 1729 (ν-(CO$_{carboxylate}$)), 1660 (ν(CO$_{amide}$)). Anal. Calcd for $C_{12}H_{16}N_2O_3$: C, 61.00; H, 6.83; N, 11.86. Found: C, 61.12; H, 6.84; N, 11.95.

*L-Phenylalanine-N-(4-pyridylcarbonyl) Methyl Ester (**L3**).* Brown oil; yield 5.42 g, 95%.[13]

General Synthesis of L4−L6. These species were prepared similarly to **L1−L3** using nicotinic acid chloride instead of isonicotinic acid chloride.

*L-Alanine-N-(3-pyridylcarbonyl) Methyl Ester (**L4**).* White solid; yield 290 mg, 69%. ^{1}H NMR (acetone-d_6): δ 9.08 (m, 1H, *H*(2)), 8.71 (m, 1H, *H*(6)), 8.23 (m, 2H, *H*(4)), 8.14 (s br, 1H, *NH*), 7.48 (m, 1H, *H*(5)), 4.66 (qd, *J* = 7.3, 7.3 Hz, 1H, NHC*H*), 3.70 (s, 3H, COOCH_3), 1.48 (d, *J* = 7.32 Hz, 3H, CHCH_3). ^{13}C NMR (acetone-d_6): δ 174.7 (COOCH$_3$), 166.8 (CONH), 1534.0 (2C, *C*(2)), 150.4 (2C, *C*(6)), 136.6 (*C*(4)), 131.6 (*C*(3)), 125.1 (2C, *C*(5)), 53.3 (NHCH), 50.3 (COOCH$_3$), 18.5 (CHCH$_3$). IR (solid, cm^{-1}): 3324 (ν(NH)), 1740 (ν(CO$_{carboxylate}$)), 1636 (ν(CO$_{amide}$)), 1524 ((ν(C═N)).

*L-Valine-N-(3-pyridylcarbonyl) Methyl Ester (**L5**).* White solid; yield 470 mg, 82%. ^{1}H NMR (acetone-d_6): δ 9.07 (m, 1H, *H*(2)), 8.70 (m, 1H, *H*(6)), 8.23 (m, 2H, *H*(4)), 7.95 (s br, 1H, N*H*), 7.47 (m, 1H, *H*(5)), 4.58 (dd, *J* = 8.4, 6.4 Hz, 1H, NHC*H*), 3.72 (s, 3H, COOCH_3), 2.26 (m, 1H, C*H*(CH$_3$)$_2$), 1.02 (dd, *J* = 8.7, 6.8 Hz, 6H, CH(CH_3)$_2$). ^{13}C NMR (Acetone-d$_6$): δ 173.8 (COOCH$_3$), 167.5 (CONH), 154.0 (2C, *C*(2)), 150.6 (2C, *C*(6)), 136.8 (*C*(4)), 131.9 (s, 2C, *C*(3)), 125.1 (s, 2C, *C*(5)), 60.1 (NHCH), 53.1 (COOCH$_3$), 32.4 (CH(CH$_3$)$_2$), 20.5 (2C, CH-(CH$_3$)$_2$), 19.8 (2C, CH(CH$_3$)$_2$). IR (solid, cm^{-1}): 3332 (ν(NH)), 1733 (ν(CO$_{carboxylate}$)), 1638 (ν-(CO$_{amide}$)), 1522 ((ν(C═N)).

dx.doi.org/10.1021/om300610j | *Organometallics* 2012, 31, 5950−5957

*L-Phenylalanine-N-(3-pyridylcarbonyl) Methyl Ester (**L6**).* Light brown oil; yield 370 mg, 66%.[13]

Synthesis of Re-1. [Re(bipy)(CO)$_3$(CF$_3$SO$_3$)] (205 mg, 0.36 mmol) and L-alanine-*N*-(4-pyridylcarbonyl) methyl ester (**L1**; 223 mg, 1.07 mmol) were stirred in dry DCM (20 mL) for 12 h at room temperature under a nitrogen atmosphere. Then, the solvent was removed under vacuum and the product was purified by an alumina chromatographic column, starting from a 70/1 mixture of the solvents DCM and MeOH and increasing the polarity until 70/5. The second yellow fraction eluted was collected, evaporated, and dried under vacuum to give complex **Re-1** as a yellow solid (75 mg, 27%). ^{1}H NMR (acetone-d_6): δ 9.49 (d, J = 5.4 Hz, 2H, C*H*(6) bipy), 8.80−8.65 (m, 4H, C*H*(3) bipy, C*H*(2) Py), 8.47 (t, J = 7.9 Hz, 2H, C*H*(4) bipy), 8.39 (s br, 1H, N*H*), 8.05−7.98 (m, 2H, C*H*(5) bipy), 7.81 (dd, J = 5.2, 1.5 Hz, 2H, C*H*(3) Py), 4.58−4.49 (m, 1H, C*H*(7)), 3.64 (s, 3H, OC*H*$_3$), 1.41 (d, J = 7.3 Hz, 3H, C*H*$_3$).^{13}C NMR (acetone-d_6): δ 196.3 (*C*O), 192.5 (*C*O), 173.1 (*C*OO), 163.9 (*C*ON), 156.9 (*C*(2) bipy), 155.0 (*C*(6) bipy), 153.9 (*C*(2) py), 145.0 (*C*(4) py), 142.4 (*C*(4) bipy), 130.0 (*C*(5) bipy), 125.9 (*C*(3) bipy), 125.4 (*C*(3) py), 52.4 (*C*H), 49.7 (O*C*H$_3$), 17.2 (*C*H$_3$). IR (solid, cm^{-1}): 2029 (s, ν(CO)), 1905 ((m, ν(CO)). Anal. Calcd for ReC$_{24}$H$_{20}$N$_4$O$_9$SF$_3$: C, 36.78; H, 2.57; N, 7.15. Found: C, 37.36; H, 2.78; N, 6.74. MS (ES): m/z calcd for C$_{23}$H$_{20}$N$_4$O$_6$Re$^+$ (M$^+$) 634.6, found 634.8.

Synthesis of Re-2. This compound was prepared similarly to **Re-1** using L-valine-*N*-(4-pyridylcarbonyl) methyl ester (**L2**) instead of L-alanine-*N*-(4-pyridylcarbonyl) methyl ester (**L1**). The pure product was obtained as a yellow solid (30% yield). ^{1}H NMR (acetone-d_6): δ 9.49 (d, J = 5.5 Hz, 2H, *H*(6) bipy), 8.79−8.67 (m, 4H, C*H*(3) bipy, C*H*(2) Py), 8.48 (ddd, J = 8.1, 2.9, 1.5 Hz, 2H, C*H*(4) bipy), 8.11 (s br, 1H, N*H*), 8.06−7.97 (m, 2H, C*H*(5) bipy), 7.80 (dd, J = 5.2, 1.5 Hz, 2H, C*H*(3) Py), 4.51−4.42 (m, 1H, C*H*(7)), 3.67 (s, 3H, OC*H*$_3$), 2.19 (dq, J = 20.2, 6.7 Hz, 2H, C*H*(8)), 0.94 (dd, J = 6.8, 2.9 Hz, 6H, 2C*H*$_3$). ^{13}C NMR (acetone-d_6): δ 197.30 (*C*O), 193.5 (*C*O), 172.2 (*C*OO), 164.7 (*C*ON), 156.9 (*C*(2) bipy), 155.0 (*C*(6) bipy), 153.8 (*C*(2) py), 145.2 (*C*(4) py), 142.4 (*C*(4) bipy), 130.1 (*C*(5) bipy), 125.9 (*C*(3) bipy), 125.5 (*C*(3) py), 59.4 (*C*H), 52.3 (O*C*H$_3$), 31.3 (*C*H$_2$), 19.4 (*C*H$_3$), 18.7 (*C*H$_3$). IR (solid, cm^{-1}): 2029 (s, ν(CO)), 1904 ((m, ν(CO)). Anal. Calcd for ReC$_{26}$H$_{24}$N$_4$O$_9$SF$_3$: C, 38.42; H, 2.95; N, 6.89. Found: C, 38.83; H, 3.32; N, 7.47. MS (ES): m/z calcd for C$_{25}$H$_{24}$N$_4$O$_6$Re$^+$ (M$^+$) 663.1, found 662.9.

Synthesis of Re-3. This compound was prepared similarly to **Re-1** using L-phenylalanine-*N*-(4-pyridylcarbonyl) methyl ester (**L3**) instead of L-alanine-*N*-(4-pyridylcarbonyl) methyl ester (**L1**). The pure product was obtained as ayellow solid (20% yield).[13]

Synthesis of Re-4. The compound was prepared similarly to **Re-1** using L-alanine-*N*-(3-pyridylcarbonyl) methyl ester (**L4**) instead of L-alanine-*N*-(4-pyridylcarbonyl) methyl ester (**L1**). The pure product was obtained as a yellow solid (272 mg, 70% yield). ^{1}H NMR (acetone-d_6): δ 9.50 (d, J = 5,4 Hz, 2H, C*H*(6) bipy), 8.87−8.80 (m, 1H, C*H*(2) py), 8.77 (d, J = 8.2 Hz, 2H, C*H*(3) bipy), 8.71 (dd, J = 5.7, 0.7 Hz, 1H C*H*(6) py), 8.65−8.52 (m, 2H, N*H*, C*H*(4) py), 8.51−8.41 (m, 2H, C*H*(4) bipy), 7.99−8.04 (m, 2H, C*H*(5) bipy), 7.56 (ddd, J = 8.0, 5.7, 0.6 Hz, 1H, C*H*(5) py), 4.51 (p, J = 7.3 Hz, 1H, C*H*(9)), 3.66 (s, 3H, OC*H*$_3$), 1.41 (d, J = 7.3 Hz, 3H, C*H*$_3$). ^{13}C NMR (acetone-d_6): δ 196.3 (*C*O), 192.4 (*C*O), 173.2 (*C*OO), 163.3 (*C*ON), 156.8 (*C*(2) bipy), 155.1 (*C*(2) py), 154.9 (*C*(6) bipy), 152.4 (*C*(6) py), 142.4 (*C*(4) bipy), 139.2 (*C*(4) py), 133.2 (*C*(3) py), 130.0 (*C*(5) bipy), 127.4 (*C*(5) py), 126.0 (*C*(3) bipy), 52.4 (*C*H), 49.6 (O*C*H$_3$), 17.2 (*C*H$_3$). IR (solid, cm^{-1}): 2029 (s, ν(CO)), 1902 ((m, ν(CO)). Anal. Calcd for ReC$_{24}$H$_{20}$N$_4$O$_9$SF$_3$: C, 36.78; H, 2.57; N, 7.15. Found: C, 37.43; H, 2.63; N, 7.34. MS (ES) m/z calcd for C$_{23}$H$_{20}$N$_4$O$_6$Re$^+$ (M$^+$) 634.6, found 634.8.

Synthesis of Re-5. This compound was prepared similarly to **Re-1** using L-valine-*N*-(3-pyridylcarbonyl) methyl ester (**L5**) instead of L-alanine-*N*-(4-pyridylcarbonyl) methyl ester (**L1**). The pure product was obtained as a yellow solid (134 mg, 70% yield). ^{1}H NMR (acetone-d_6): δ 9.50 (d, J = 5.4 Hz, 2H, C*H*(6) bipy), 8.84−8.74 (m, 4H, C*H*(3) bipy, C*H*(2,6) py), 8.54−8.44 (m, 3H, C*H*(4) bipy, C*H*(4) py), 8.00−8.07 (m, 3H, C*H*(5) bipy, N*H*), 7.60 (ddd, J = 8.0, 5.8, 0.5 Hz, 1H, C*H*(5) py), 4.44 (dd, J = 8.3, 6.4 Hz, 1H, C*H*(9)), 3.71 (s, 3H, OC*H*$_3$), 2.19 (dq, J = 13.5, 6.8 Hz, 1H, C*H*(10)), 0.95 (dd, J = 6.8, 5.1 Hz, 6H, 2C*H*$_3$). ^{13}C NMR (acetone-d_6): δ 196.3 (*C*O), 192.3 (*C*O), 172.3 (*C*OO), 164.2 (*C*ON), 156.9 (*C*(2) bipy), 155.3 (*C*(2) py), 154.9 (*C*(6) bipy), 152.2 (*C*(6) py), 142.5 (*C*(4) bipy), 139.3 (*C*(4) py), 133.6 (*C*(3) py), 130.1 (*C*(5) bipy), 127.5 (*C*(5) py), 126.0 (*C*(3) bipy), 59.4 (*C*HN), 52.3 (O*C*H$_3$), 31.2 (*C*H), 19.4 (*C*H$_3$), 18.8 (*C*H$_3$). IR (solid, cm^{-1}): 2029 (s, ν(CO)), 1904 ((m, ν(CO)). Anal. Calcd for ReC$_{26}$H$_{24}$N$_4$O$_9$SF$_3$: C, 38.42; H, 2.95; N, 6.89. Found: C, 38.76; H, 3.11; N, 7.08. MS (ES): m/z calcd for C$_{25}$H$_{24}$N$_4$O$_6$Re$^+$ (M$^+$) 663.1, found 662.8.

Synthesis of Re-6. This compound was prepared similarly to **Re-1** using L-phenylalanine-*N*-(3-pyridylcarbonyl) methyl ester (**L6**) instead of L-alanine-*N*-(4-pyridylcarbonyl) methyl ester (**L1**). The pure product was obtained as a yellow solid (330 mg, 90% yield).[13]

RESULTS AND DISCUSSION

Synthesis of Ligands and Complexes. Pyridyl-amino acid derivatives **L1**−**L6** were synthesized by reaction of either, commercially available isonicotinic acid chloride or nicotinic acid chloride with the corresponding amino acid methyl ester derivative in presence of triethylamine to assist the condensation reaction (Scheme 1). Infrared spectroscopy showed

Scheme 1. Depiction of Selected Ligands and Their Precursors

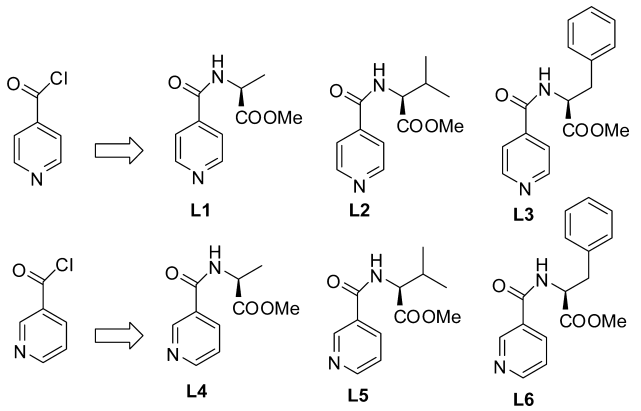

the displacement of the ν(CO$_{acyl}$) band from ca. 1750 cm^{-1} to a ν(CO$_{amide}$) band at ca. 1650 cm^{-1}, indicating the successful condensation reaction. Synthesis of the cationic rhenium derivatives **Re-1**−**Re-6** (see Table 1) was achieved by following

Table 1. Numbering Scheme for the Synthesized Rhenium Species

	AA derivative		
	Ala	Val	Phe
para-Re species	**Re-1**	**Re-2**	**Re-3**
meta-Re species	**Re-4**	**Re-5**	**Re-6**

literature precedents.[4] This involved initial formation of rhenium tricarbonyl bipyridyl chloride and then activation of the chloride by exchange to triflate to allow its final displacement for the desired pyridyl derivative **L1**−**L6** under mild conditions (Scheme 2). Spectroscopic characterization of each ligand and rhenium complex was performed using IR, ^{1}H and ^{13}C NMR, and UV−vis. Infrared spectra of rhenium complexes **Re-1**−**Re-6** showed two bands corresponding to the ν(CO) symmetric and asymmetric stretching modes at ca. 2029 (s) and 1904 (br) cm^{-1}, respectively, which are typical of these

dx.doi.org/10.1021/om300610j | *Organometallics* 2012, 31, 5950−5957

Scheme 2. Synthesis of Rhenium Complexes Re-1−Re-6[a]

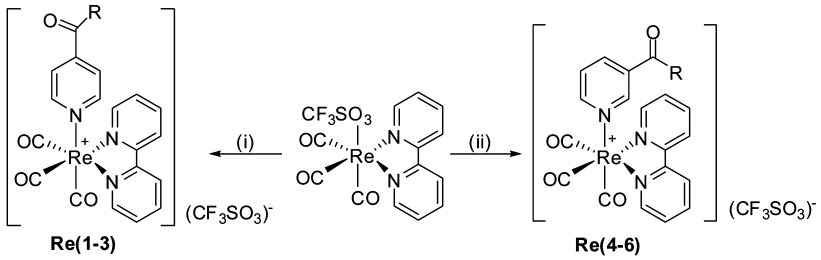

R: L-alanine methyl ester (**Re-1**, **Re-4**)
L-valine methyl ester (**Re-2**, **Re-5**)
L-phenyl alanine methyl ester (**Re-3**, **Re-6**)

[a]Legend: (i) **L1−L3**, DCM, room temperature, 12 h, argon atmosphere; (ii) **L4−L6**, DCM, room temperature, 12 h, argon atmosphere.

types of cationic species with C_{3v} symmetry. The higher energy band arises from an A_1 mode, whereas the lower energy band, a broad band, is due to an E mode.[14] Moreover, ^{1}H NMR spectra in acetone-d_6 showed, in all cases, a characteristic low-field shift of the bipyridine protons $H(6)$, from 9.0 to 9.5 ppm, indicative of the successful displacement of the triflate ligand for the pyridine derivatives **L1−L6**. Further analytical data for each complex were provided through elemental analysis and mass spectroscopy, which corroborate the accomplishment of the synthesis of the bioconjugated rhenium(I) species **Re-1−Re-6**. Additionally, crystals of **Re-2** and **L2** suitable for X-ray analysis (SHELX programs) were obtained by slow evaporation of a CH_3OH solution and slow diffusion of a mixture of acetone and hexane, respectively.

Luminescence Properties of Complexes. The electronic spectra of species **Re-1−Re-6** were recorded in DCM solution and showed the typical characteristics associated with bis-imine Re(I) derivatives: i.e., two common features, ligand-centered transitions (bipyridine, pyridine) at higher energy (<320 nm) and metal to ligand charge-transfer transitions (^{1}MLCT) at lower energy (345−360 nm). Specifically, the complexes **Re-4−Re-6**, derived from the *meta*-substituted ligands, have a slightly red-shifted ^{1}MLCT transition in comparison to the *para* analogues (see Figure 1), indicating that the main orbitals implicated in the transition are those belonging to Re(dπ) and bipy(π^*), whereas some contribution from the pyridine-based orbitals is assumed in **Re-1−Re-3**. Relevant spectroscopic data are given in Table 2. Direct irradiation of the ^{1}MLCT bands using excitation wavelengths between 350 and 410 nm gave a structureless visible emission centered at ca. 537 nm in the case

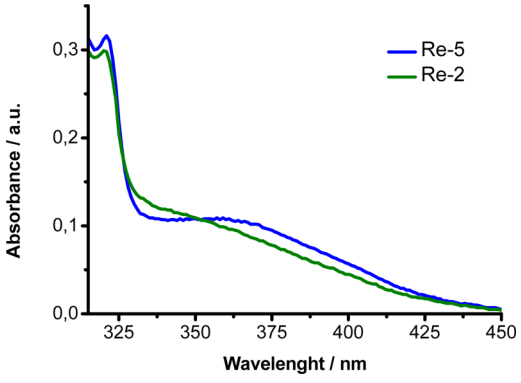

Figure 1. UV-absorption spectra for complexes **Re-2** and **Re-5** in DCM at 298 K.

Table 2. Photophysical Data of Complexes Re-1−Re-6 in Degassed Solutions of DCM and CH_3CN at 298 K

complex	λ_{exc}/ nm	λ_{em}/ nm	τ_{MLCT}/ ns[a]	λ_{abs}(^{1}MLCT)/nm (ε/dm^3 mol^{-1} cm^{-1})
Re-1	401	537	320	351 (4200)
Re-2	366	538	374	352 (6720)
		553[b]	151[b]	
Re-3	358	537	327	348 (4320)
Re-4	371	540	267	355 (4280)
		554[b]	146[b]	
Re-5	417	541	374	359 (4360)
		553[b]	140[b]	
Re-6	410	540	370	359 (3960)

[a]Degassed DCM solution. [b]Degassed CH_3CN solution

of complexes **Re-1−Re-3** and at ca. 540 nm for **Re-4−Re-6**, and thus, once again, a small red shift was observed on going from *para* rhenium derivatives to *meta* rhenium derivatives (Figure 2). Such features are typical of cationic bis-imine Re(I)

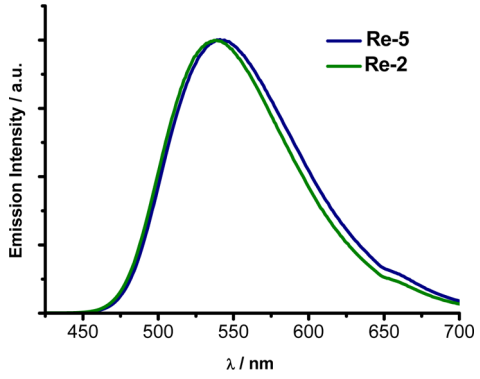

Figure 2. Emission spectra for complexes **Re-2** and **Re-5** in degassed DCM at 298 K.

complexes, where the emission is frequently assigned as long-lived ^{3}MLCT in origin, specifically dπ(Re) → π^*(bipy). Luminescent lifetime measurements of each complex performed in degassed DCM showed a good fitting to a single exponential (indicative of one excited state environment) in the 267−374 ns domain, consistent with phosphorescent emission from a ^{3}MLCT state for complexes of the type *fac*-[Rebipy(CO)$_3$(L)]$^+$.[15] The longer lifetimes observed in DCM in comparison with those reported in the literature for similar complexes in CH_3CN ($\tau \approx$ 100−200 ns) can be rationalized in

dx.doi.org/10.1021/om300610j | *Organometallics* 2012, 31, 5950−5957

terms of the greater stabilization of MLCT excited state in polar solvents: i.e., lowering the MLCT excited state energy allows nonradiative processes to occur easily.[16] Further lifetime data were recorded in CH_3CN solution for species **Re-2**, **Re-4**, and **Re-5**. Lifetime values are in the range of 140−150 ns, which corroborate the hypothesis of a greater MLCT excited state stabilization (see Table 2). As expected, maxima emission wavelength in CH_3CN solution were also shifted from ca. 539 to ca. 553 nm, in accordance with the greater stabilization of the excited state in polar solvents.

X-ray Crystallography. Ligand **L2** crystallized in space group $P2_12_12_1$ with a single molecule per asymmetric unit (Figure 3). Selected bond distances and angles are collected in

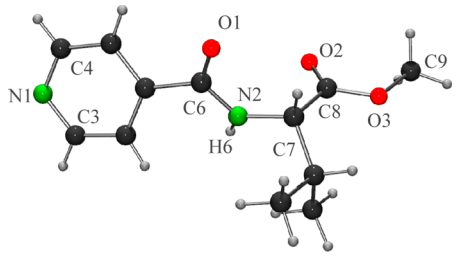

Figure 3. Ortep representation of ligand **L2**.

Table 3. Selected Bond Lengths (Å) and Angles (deg) for L2

C(1)−C(6)	1.508(2)	C(6)−N(2)	1.345(2)
C(6)−O(1)	1.2263(18)	N(2)−C(7)	1.452(2)
O(1)−C(6)−N(2)	123.88(14)	N(2)−C(6)−C(1)	115.88(13)
O(1)−C(6)−C(1)	120.23(14)	C(6)−N(2)−C(7)	121.09(13)

Table 3. Structural parameters showed normal values. Additionally, **L2** displayed an intermolecular, short, and reasonably linear H bond (H6···N1# (#: $-x + 2$, $y - {}^1/_2$, $-z + {}^1/_2$) = 2.24(2) Å; N2−H6···N1 = 168.6(16)°) between the N−H amide group and the pyridinic N atom of one adjacent molecule. Such a strong interaction led to an infinite chain of molecules (see Figure S1 in the Supporting Information).

Complex **Re-2** crystallized in space group $P2_1/c$ with two rhenium complexes per asymmetric unit (see Table S1 in the Supporting Information); these two molecules differ slightly in angles and bond distances. The coordination sphere of each rhenium unit can be described as a slightly distorted octahedron in which the three carbonyl ligands are arranged in a facial geometry (Figure 4). In both cases, the equatorial plane is described by the chelate bipyridine ligand and two *trans* carbonyls. A third carbonyl and the pyridine derivative are placed in the apical plane. Deviation from an ideal octahedron mostly originates from the geometric restraints imposed by the chelated ligand, with chelate angles of N(1)−Re(1)−N(2) = 75.70(4)° and N(5)−Re(2)−N(6) = 75.65(7)° instead of the ideal 90°, and a slight deviation from planarity (torsion angles N(1)−C(5)−C(6)−N(2) = 2.7(2)° and N(5)−C(35)−C(36)−N(6) = 2.4(3)° as a result of packaging forces). Both of them showed a pair of mutual N−H···O close contacts (H4A··· O12# (#: x, $y - 1$, z) = 2.228 Å, N4−H4A··· O12 = 155.14° and H8A···O6# (#: x, $y + 1$, z) = 2.042 Å, N8−H8A···O6 = 169.99°) between the NH of one complex and the oxygen of the carbonyl methyl ester derivative of an adjacent molecule, indicative of mutual hydrogen bonding (Figure 5). As

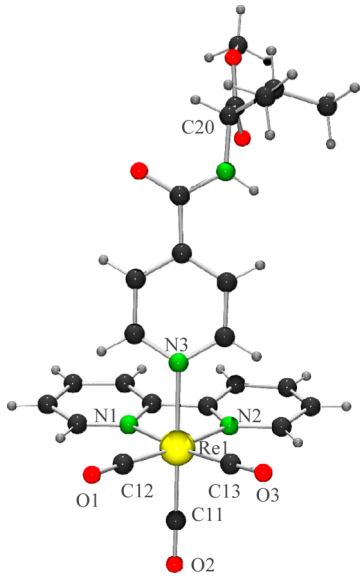

Figure 4. Ortep representation of complex **Re-2** (the second molecule within the asymmetric unit and the counterions were omitted for clarity). The most relevant bond lengths (Å) and angles (deg): Re(1)−C(11) = 1.912(14), Re(1)−C(13) = 1.924(15) , Re(1)−C(12) = 1.933(11), Re(1)−N(1) = 2.127(12), Re(1)−N(2) = 2.156(10), Re(1)−N(3) = 2.187(9); N(1)−Re(1)−N(2) = 75.7(4), C(11)−Re(1)−N(3) = 175.3(4), C(11)−Re(1)−C(13) = 88.9(5), C(11)−Re(1)−C(12) = 87.4(5), C(12)−Re(1)−N(1) = 99.3(4), C(11)−Re(1)−N(2) = 95.4(5).

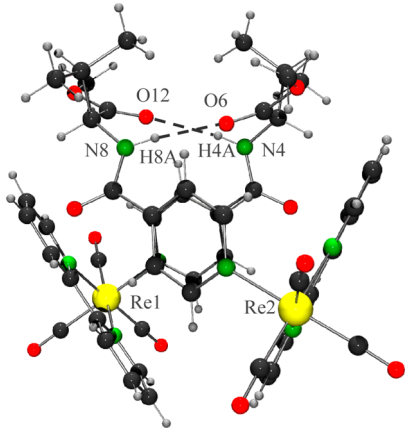

Figure 5. Ortep representation of adjacent molecules of complex **Re-2** showing the N−O interaction (- - -).

expected, the asymmetric carbon atoms, C25 and C50, retained the *S* configuration of the commercial valine methyl ester used in the synthesis of **L2**. In addition, bond lengths and angles were within the expected range for analogous complexes reported in the literature (see legend in Figure 4).[4,17]

Cellular Studies and Confocal Microscopy. Having established that complexes **Re-1**−**Re-6** possessed the required photophysical properties for application in fluorescent cell imaging, a series of experiments were undertaken in which they were incubated with MCF-7 (human adenocarcenoma) cells. Incubation was performed at 4 °C to suppress active transport uptake mechanisms and to prevent encapsulation in endosomes. Following incubation and washing to remove the agent from the medium, the cells were allowed to attain ambient temperature to grant biological processes to reactivate and to

dx.doi.org/10.1021/om300610j | *Organometallics* 2012, 31, 5950−5957

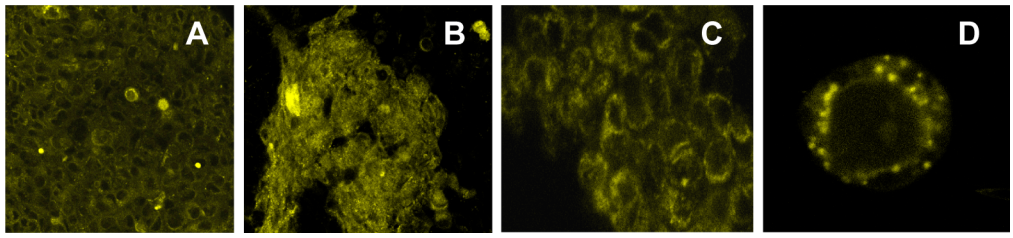

Figure 6. Cell imaging with complexes **Re-1**−**Re-3** showing clustering (A−C, respectively) and cell imaging with complex **Re-2** showing localization (D).

permit cellular distribution mechanisms to operate. The results of the cell imaging experiments demonstrate that small changes in ligand structure can have a vital role in the biological properties of imaging agents. While the analogous pairs of agents from the series of complexes **Re-1**−**Re-3** and **Re-4**−**Re-6** bear identical substituents, and thus have similar solubilities, lipophilicities, etc., their behavior in the cell experiments was markedly different. Whereas the pairs of complexes each showed good uptake, the effect on the cells was dramatically different: *para*-substituted analogues **Re-1**−**Re-3** had a dramatic effect on the cells, with the cell structure being badly damaged and clustering of dead and dying cells being observed in all cases (see Figure 6A−C). Although a small number of cells showed healthy structures and the typical pattern of localization of monocationic Re complexes with some general cytoplasmic staining and more intense mitochondrial localization (see Figure 6D), the bulk of the populations were damaged and clustered, indicating that these complexes have limited use as imaging agents.

In addition, these samples showed considerable photobleaching, with *z* stacking being impossible due to the loss of image intensity upon irradiation. Interestingly, the only previous report of significant damage to cell morphology across an entire cell sample and associated photobleaching was in the first published article dealing with the application of rhenium bipyridines in cell imaging and was restricted to the case of a chloride complex.[18] In this case both the toxicity and photobleaching were assigned to the lability of the halide, allowing interaction with biological donors, and subsequent photoreactivity upon irradiation. While there are many reports of variations in cytotoxicity of rhenium tricarbonyl bipyridine-pyridine complexes, the levels of cytotoxicity are always low, and the only case in which essentially quantitative cell death has occurred is the chloride complex mentioned above. Given the number of examples now reported of such complexes applied in imaging experiments which show low levels of cyctotoxicity and photobleaching, and the similarity observed here with the quantitative cell death seem with the labile halide species, it is likely that the toxicity and photobleaching detected with **Re-1**−**Re-3** may be a function of lability, and especially photolability of the pyridine ligands **L1**−**L3** in the biological environment.

In contrast, the *meta*-substituted analogues showed the same good levels of uptake, with patterns of localization similar to in the cells which had survived the treatment with the *para* analogues, but in these cases the cell samples remained healthy, with no clustering and no significant photobleaching and phototoxicity. The patterns of uptake show a trend which can be explained in terms of lipophilicity, as would be expected for a passive uptake mechanism, with the most highly substituted phenyl alanine analogue **Re-6** (see Figure 7D) showing the most intense luminescence and the alanine and valine

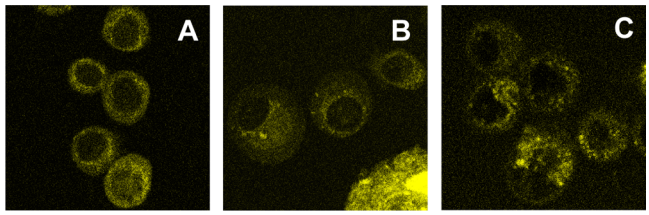

Figure 7. Cell imaging with complexes **Re-4**−**Re-6** showing localization (A−C, respectively).

derivatives showing similar lower levels of intensity (see Figure 7A,B, respectively). The patterns of localization are reminiscent of the now well-established patterns observed with monocationic, lipophilic rhenium complexes. In these cases, a general cytoplasmic staining along with more intense mitochondrial and occasional nucleolar localization was observed.

Given this dramatic difference between the cellular behavior of two apparently closely related sets of complexes, a series of experiments were undertaken to probe the mechanism behind their behaviors. NMR studies showed that while ligand displacement occurred in both series of complexes under unnatural conditions ($CDCl_3$ and CH_3CN, with competing pyridine ligands) and under conditions which matched those of the incubation experiments ($DMSO/D_2O$ with or without competing ligands), no loss of the axial pyridine was observed in either the *para* or *meta* series under physiological conditions; indeed, to observe any ligand exchange at all, high temperature was required. These different rates of ligand exchange in solvents of different polarities can be attributed to differing degrees of solvation of the incoming ligands. It has previously been observed that chloride can displace coordinated pyridines from rhenium *fac* tricarbonyl complexes,[4b] in organic solvents; however, this does not occur in aqueous media. Also, it has been shown that an associative mechanism is likely to be at play in these cases;[19] therefore, the nucleophilicity of the incoming ligand is crucial to the rate of displacement. Therefore, aqueous media which will allow hydrogen bond donation to the pyridine nitrogen (or other donor atoms) greatly retard the rate of ligand exchange. Thus, it appears unlikely that the exchange of ligands in the *para* series occurs during the incubation, and indeed the similar levels of uptake argue against this possibility, as had an aqua complex (the product of loss of pyridine in any water-containing medium) been formed, this more polar species would have not shown uptake similar to that of the *meta* series. Therefore, it seems reasonable that the assumed lability of the *para* series, which is correlated with the observed destruction of cells, is induced in the cells by an as yet unknown mechanism. The photobleaching observed with the *para* series is again unusual and by analogy with the halide example could indicate photolability of the axial pyridine and thus toxicity. However, it is unlikely that phototoxicity alone can explain the

dx.doi.org/10.1021/om300610j | *Organometallics* 2012, 31, 5950−5957

Scheme 3. Depiction of Intramolecular Electron Shuttling for Para and Meta Rhenium Analogues, Respectively

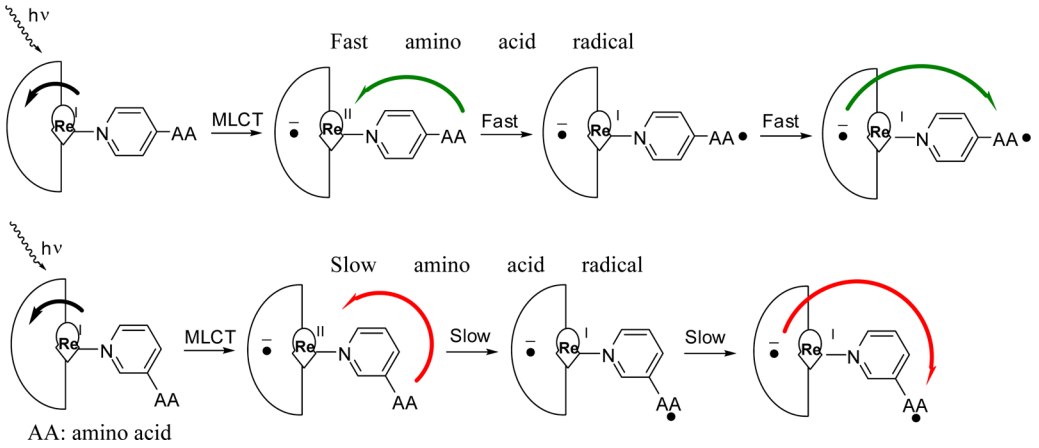

unusual images observed with the *para* series, unless the phototoxicity is extremely rapid, as the first images collected showed deformed cells.

A rationalization of these phenomena could be achieved by consideration of the ease of amino acid radical formation: i.e., metal-to-ligand charge transfer excited states of metal complexes can be used to initiate amino acid redox processes. The rate for radical generation can be accelerated by increasing the oxidizing strength of quenched product and also by facilitating the processes by which electrons move along the species: i.e., electron transfer (ET) and photoinduced electron transfer.[20] Along that line, and on the basis of studies reported by Nocera et al., who demonstrated that tyrosine oxidation using MLCT excited states of rhenium polypyridyl complexes takes place more easily when intramolecular electron shuttling occurs via a unidirectional electron cascade,[21] *para* derivatives should increase this effect over *meta* derivatives. In general, *para* derivatives allow an easier electronic communication between the metal center and the *para* substituent, and thus, formation of amino acid radicals would be prompted in those species (Scheme 3). The radical fragment could possibly interact with any endogenous donor, and the displacement of the axial pyridine would take place easily. These hypotheses are in accord with the fact that *para* derivatives suffer photobleaching in vivo as well as provoke cellular death in all cases, and none of these effects are observed for their *meta* analogues. Furthermore, it was tested that there is no evidence from prolonged irradiation in a spectrometer of the photodestruction of the *para* series. Such an observation would suggest that a mechanism which involves, rather than intramolecular photolabilization of the axial pyridine, an intermolecular photoinduced reaction between the excited state of the complexes and an as yet unidentified biological species would also be feasible. This could involve phototoxicity induced by simple radical generation via electron transfer from an endogenous residue, for instance a tyrosine, to the complex. While the exact mechanism of the toxicity of the *para* series both is unclear and apparently involves reaction with complex biological molecules, as it could not be reproduced in vitro, the dramatic difference in behavior between the *para* and *meta* series demonstrates, again, that apparently small changes in the structures of rhenium complexes can induce profound changes in cellular behavior.

CONCLUSIONS

In summary, we have reported the synthesis of a series of *para* and *meta* pyridyl amino acid derivatives and their coordination to *fac*-[Re(bipy)$(CO)_3$] units. Photophysical studies of the novel rhenium species showed the typical values for these type of cationic derivatives: i.e., emission intensity maxima between 537 and 541 nm, large Stokes shifts (>140 nm), and long lifetimes (270−370 ns). Cell imaging experiments were undertaken using the MCF-7 cell line and *para* and *meta* rhenium derivatives, which showed a good uptake in both cases but a markedly different effect on the cells. The *para*-substituted analogues **Re-1**−**Re-3** induced damage in the cell structure, and cell death was observed in all cases. The typical localization pattern of monocationic Re complexes, i.e. cytoplasmic staining and more intense mitochondrial localization, was observed for a small percentage of healthy cells before undergoing photobleaching. In contrast, cells incubated with the *meta*-substituted analogues **Re-4**−**Re-6** remained healthy with no clustering and no significant photobleaching and phototoxicity and showed the typical localization pattern for monocationic Re complexes. The different behavior in vivo for both sets of rhenium complexes can be rationalized by the ease of amino acid radical formation in the case of *para* rhenium derivatives in comparison with their *meta* rhenium analogues. Upon irradiation of the imaging agent, a rapid process of intramolecular and unidirectional shuttling of electrons could be crucial to induce the formation of amino acid radicals in the case of *para* rhenium derivatives. Formation of radicals within the cell imaging agent would favor their interaction with endogenous donors. Exchange processes involving the axial pyridine might occur at this point and, thus, translate into the higher toxicity and photobleaching associated with those species. Alternatively, an intermolecular photoinduced reaction between the excited state of the complexes and an as yet unidentified biological species could also not be discarded. Nevertheless, it is evident that small structural changes in rhenium complexes can induce profound variation in cellular behavior.

ASSOCIATED CONTENT

Supporting Information

A table, figure, and CIF files giving X-ray crystallographic data for **L2** and **Re-2** and another view of **L2**. This material is available free of charge via the Internet at http://pubs.acs.org.

dx.doi.org/10.1021/om300610j | *Organometallics* 2012, 31, 5950−5957

AUTHOR INFORMATION

Corresponding Author

*E-mail: gimeno@unizar.es.

Notes

The authors declare no competing financial interest.

ACKNOWLEDGMENTS

We thank the Ministerio de Economía y Competitividad (MEC/FEDER CTQ2010-20500-C02-01) for financial support. We also thank Prof. David Lloyd and Dr. Anthony J. Hayes for their comments and help with the cell imaging experiments performed at the Confocal Microscopy Unit at Cardiff School of Biosciences.

REFERENCES

(1) (a) Fernández-Moreira, V.; Thorp-Greenwood, F. L.; Coogan, M. P. *Chem. Commun.* **2010**, *46*, 186. (b) Zhao, Q.; Huang, C.; Li, F. *Chem. Soc. Rev.* **2011**, *40*, 2508. (c) Balasingham, R. G.; Coogan, M. P.; Thorp-Greenwood, F. L. *Dalton Trans.* **2011**, *40*, 11663. (d) Lo, K. K.-W.; Chio, A. W.-T.; Law, W. H.-T. *Dalton Trans.* **2012**, *41*, 6021.

(2) (a) Worl, L. A.; Duesing, R.; Chen, P.; Della Ciana, L.; Meyer, T. J. *J. Chem. Soc., Dalton Trans.* **1991**, 849. (b) Stufkens, D. J.; Vlček, A., Jr. *Coord. Chem. Rev.* **1998**, *177*, 127. (c) Sacksteder, L. A.; Lee, M.; Demas, J. N.; DeGraff, B. A. *J. Am. Chem. Soc.* **1993**, *115*, 8230.

(3) For a comprehensive and authoritative review of issues related to fluorescence, see: Lakowicz, J. R. *Principles of Fluorescence Spectroscopy*, 3rd ed.; Springer: New York, 2006.

(4) (a) Fernández-Moreira, V.; Thorp-Greenwood, F. L.; Amoroso, A. J.; Cable, J.; Court, J. B.; Gray, V.; Hayes, A. J.; Jenkins, R. L.; Kiriuki, B. M.; Lloyd, D.; Millet, C. O.; Williams, C. F.; Coogan, M. P. *Org. Biomol. Chem.* **2010**, *8*, 3888. (b) Amoroso, A. J.; Arthur, R. J.; Coogan, M. P.; Court, J. B.; Fernández-Moreira, V.; Hayes, A. J.; Lloyd, D.; Millet, C. O.; Pope, J. A. *New J. Chem.* **2008**, *32*, 1097.

(5) (a) Lo, K. K.-W.; Zhang, K. Y.; Chung, C.-K.; Kwok, K. Y. *Chem. Eur. J.* **2007**, *13*, 7110. (b) Puckett, C. A.; Barton, J. K. *J. Am. Chem. Soc.* **2009**, *131*, 8738. (c) Puckett, C. A.; Barton, J. K. *Bioorg. Med. Chem.* **2010**, *18*, 3564.

(6) (a) Lo, K. K.-W.; Hui, W.-K.; Ng, D. C.-M. *J. Am. Chem. Soc.* **2002**, *124*, 9344. (b) Lo, K. K.-W.; Lee, T. K.-M. *Inorg. Chem.* **2004**, *43*, 5275. (c) Lo, K. K.-W.; Lau, J. S.-Y. *Inorg. Chem.* **2007**, *46*, 700.

(7) (a) Stephenson, K. A.; Banerjee, S. R.; Besenger, T.; Sogbein, O. O.; Levadala, M. K.; McFarlane, N.; Lemon, J. A.; Boreham, D. R.; Maresca, K. P.; Brennan, J. D.; Babich, J. W.; Zubieta, J.; Valliant, J. F. *J. Am. Chem. Soc.* **2004**, *126*, 8598. (b) Ferri, E.; Donghi, D.; Panigati, M.; Precipe, G.; D'Alfonso, L.; Zanoni, I.; Baldoli, C.; Maiorana, S.; D'Alfonso, G.; Lincandro, E. *Chem. Commun.* **2010**, *46*, 6255. (c) Raszeja, L.; Maghnouj, A.; Hahn, S.; Metzler-Nolte, N. *ChemBioChem* **2011**, *12*, 371.

(8) (a) Viola-Villegas, N.; Rabideau, A. E.; Cesnavicious, J.; Zubieta, J.; Doyle, R. P. *ChemMedChem* **2008**, *3*, 1387. (b) Vortherms, A. R.; Kahkoska, A. R.; Rabideau, A. E.; Zubieta, J.; Andersen, L. L.; Madsen, M.; Doyle, R. P. *Chem. Commun.* **2011**, *47*, 9792.

(9) Lo, K. K.-W.; Louie, M.-W.; Sze, K.-S.; Lau, J. S.-Y. *Inorg. Chem.* **2008**, *47*, 602.

(10) Josefsen, L. B.; Boyle, R. W. *Met.-Based Drugs* **2008**, *24*, 276109. (b) Stochel, G.; Wanat, A.; Kulís, E.; Stasicka, Z. *Coord. Chem. Rev.* **1998**, *171*, 203.

(11) Sheldrick, G. M. *Acta Crystallogr.* **2008**, *A64*, 112.

(12) Wang, Y.; Lucia, L. A.; Schanze, K. S. *J. Phys. Chem.* **1995**, *99*, 1961.

(13) Blanco-Rodríguez, A. M.; Towrie, M.; Súkora, J.; Zálïs, S.; Vlček., A., Jr. *Inorg. Chem.* **2011**, *50*, 6122.

(14) Dattelbaum, D. M.; Omberg, K. M.; Schoonover, J. R.; Martin, R. L.; Meyer, T. J. *Inorg. Chem.* **2002**, *41*, 6071.

(15) Uppal, B. S.; Booth, R. K.; Ali, N.; Lockwood, C.; Rice, C. R.; Elliott, P. I. P. *Dalton Trans.* **2011**, *40*, 7610.

(16) (a) Kuimova, M. K.; Alsindi, W. Z.; Blake, A. J.; Davies, E. S.; Lampus, D. J.; Matousek, P.; McMaster, J.; Parker, A. W.; Towrie, M.; Sun, X.-Z.; Wilson, C.; George, M. W. *Inorg. Chem.* **2008**, *47*, 9857. (b) Sacksteder, L. A.; Lee, M.; Demas, J. N.; DeGraff, B. A. *J. Am. Chem. Soc.* **1993**, *115*, 8230.

(17) (a) Wu, S.-H.; Abruña, H. D.; Zhong, Y.-W. *Organometallics* **2012**, *31*, 1161. (b) Gómez, E.; Huertos, M. A.; Pérez, J.; Riera, L.; Menéndez-Velazquez, A. *Inorg. Chem.* **2010**, *49*, 9527. (c) Partyka, D. V.; Deligonul, N.; Washington, M. P.; Gray, T. G. *Organometallics* **2009**, *28*, 5837.

(18) Amoroso, A. J.; Coogan, M. P.; Dunne, J. E.; Fernández-Moreira, V.; Hess, J. B.; Hayes, A. J.; Lloyd, D.; Millet, C. O.; Pope, J. A.; Williams, C. *Chem. Commun.* **2007**, 3066.

(19) Fernández-Moreira, V.; Thorp-Greenwood, F. L.; Arthur, R. J.; Kiauri, B. M.; Jenkins, R. L.; Coogan, M. P. *Dalton Trans.* **2010**, *39*, 7493.

(20) (a) Reece, S. Y.; Seyedsayamdost, M. R.; Stubbe, J. A.; Nocera, D. G. *J. Am. Chem. Soc.* **2006**, *128*, 13654. (b) Ishikita, H.; Soudackov, A. V.; Hammes-Schiffer, S. *J. Am. Chem. Soc.* **2007**, *129*, 11146.

(21) Reece, S. Y.; Nocera, D. G. *J. Am. Chem. Soc.* **2005**, *127*, 9448.